Multivariable Loop-Shaping in Bilateral Telemanipulation

Kevin B. Fite
Michael Goldfarb

Department of Mechanical Engineering
Vanderbilt University
Nashville, TN 37235

Abstract

This paper presents an architecture and control methodology for obtaining transparency and stability robustness in a multivariable bilateral teleoperator system. The work presented here extends a previously published single-input, single-output approach to accommodate multivariable systems. The extension entails the use of impedance control techniques, which are introduced to render linear the otherwise nonlinear dynamics of the master and slave manipulators, in addition to a diagonalization multivariable loop shaping technique, used to render tractable the multivariable compensator design. A multivariable measure of transparency is proposed based on the relative singular values of the environment and transmitted impedance matrices. The approach is experimentally demonstrated on a three degree-of-freedom scaled telemanipulator pair with a highly coupled environment. Using direct measurement of the power delivered to the operator to assess the system's stability robustness, along with the proposed measure of multivariable transparency, the loop-shaping compensation is shown to improve the stability robustness by a factor of two and the transparency by more than a factor of five.

1 Introduction

Bilateral teleoperation systems provide for human interaction with an environment while alleviating the necessity of direct contact between the two. Using a pair of robot manipulators, such a system enables dexterous human manipulation in remote, hazardous, or otherwise inaccessible environments. Bilateral telemanipulators can additionally incorporate power attenuation or amplification between the human operator and environment, allowing for human manipulation of microscopic objects (in the case of macro-micro bilateral telemanipulation) or large-scale objects (in the case of man-amplifiers). The teleoperative performance can be characterized by the transparency, which is a measure of the extent to which the telemanipulation system presents the undistorted dynamics of the environment to the human operator. A common goal in the control of bilateral telemanipulation is to provide transparent teleoperation while ensuring the robust stability of the human-telemanipulator-environment loop.

2 Prior Work

Several researchers have investigated aspects of transparency and stability in telemanipulation, primarily through the use of two-port network modeling techniques. Hannaford [1], Yokokohji and Yoshikawa [2], and Lawrence [3] collectively proposed the use of two-port hybrid parameters to address teleoperative transparency and passivity concepts to ensure the system's stability robustness. Due to the nature of the hybrid parameter/passivity approach, no significant distinction exists between single-input single-output (SISO) and multivariable (MIMO) controller design. Because of the limited availability of MIMO analysis tools, however, few publications on bilateral telemanipulation have explicitly treated multivariable or multi-degree-of-freedom systems. Some prior works that do treat such systems include those by Colgate [4],

Itoh et al. [5], and Hashtrudi-Zaad and Salcudean [6]. Specifically, Colgate utilized the structured singular value, a multivariable frequency-domain stability robustness tool proposed by Doyle [7], to assess the stability of a macro-micro bilateral telemanipulator interacting with a passive human operator and environment. Though the telemanipulator itself was a single-degree-of-freedom system, the human-teleoperator-environment interaction was formulated in a manner that required multivariable tools in order to assess stability robustness. Colgate did not explicitly treat transparency, but instead utilized impedance shaping to intentionally alter the dynamics as perceived by the human operator through the telemanipulator. Itoh et al. experimentally implemented a six degree-of-freedom telemanipulator using passivity theory to address stability robustness, but instead of providing transparency, the telemanipulator was controlled to exhibit a task-oriented dynamic behavior specified in order to facilitate a particular telemanipulation task. Hashstrudi-Zaad and Salcudean theoretically assessed the performance and stability robustness of a three degree-of-freedom telemanipulator by incorporating a parallel force/position control to linearize and decouple the manipulators, and by assuming the human operator and environment to be decoupled, in which case the analysis reduces to that required for three decoupled single-degree-of-freedom systems.

In contrast to the combined hybrid parameter/passivity based approach, the architecture proposed by Fite et al. [8] formulates the teleoperation system as a single feedback loop to which the tools of classical control theory can then be applied to address the performance and stability robustness. In so doing, the stability robustness of the system is addressed in a non-conservative manner, and the transparency is addressed only in the bandwidth of interest. This loop shaping approach was developed in a single input, single output context; since telemanipulation

applications generally involve systems with coupled multiple degrees of freedom, however, such a method is of limited utility without extension to the multivariable case. As such, the work presented in this paper extends this previously published approach to the multivariable case of telemanipulation. Specifically, the extension entails the use of impedance control techniques to render linear the otherwise nonlinear dynamics of the master and slave manipulators, and employs a diagonalization multivariable loop shaping technique used to render tractable the multivariable loop shaping compensator design. A multivariable measure of transparency is additionally proposed based on the relative singular values of the environment and transmitted impedance matrices.

3 Multivariable Telemanipulation Architecture

Fig. 1 depicts the general notion of two-channel bilateral telemanipulation, in which a human operator interacts with a force-controlled master manipulator, which is in turn coupled to a position-controlled slave manipulator interacting with an environment. The two subsystems are coupled through scaled motion and force communication channels, where $\mathbf{C}_1$ and $\mathbf{C}_2$ represent the motion and force scaling matrices, respectively. The human motion vector from the master/human subsystem, X_h, is the combined effect of human voluntary motion and the "feedthrough" motion from the teleoperator loop. The latter is a filtered version of the motion vector filtered by the dynamics of the loop. Noting that motion at the master/human interface can result either from a human voluntary motion input vector (X_{hv}) or the teleoperation feedthrough force vector (F_h), the human arm dynamics can be written in transfer function matrix form as:

$$X_h = \begin{bmatrix} \mathbf{G_{hv}} & \mathbf{G_m} \end{bmatrix} \begin{bmatrix} X_{hv} \\ F_h \end{bmatrix} \tag{1}$$

where X_h is the motion of the human hand, X_{hv} is the voluntary input command of the human operator (e.g., a neural command), F_h is the force commanded to the master manipulator by the teleoperation loop, and the transfer function matrices $\mathbf{G_{hv}}$ and $\mathbf{G_m}$ describe the dynamic relationships between the voluntary input command vector and the master manipulator force vector, respectively, and the resulting motion at the master/human interface.

The dynamics of the slave/environment interaction are represented by the block diagrams of Figs. 2*a* and 2*b*. In the figures, $\mathbf{Z_e}$, $\mathbf{Y_s}$, and $\mathbf{C_s}$ are transfer function matrices governing the multivariable environment impedance, the admittance of the slave manipulator, and the position controller of the slave manipulator, respectively, and $\widetilde{\mathbf{G}}_s$ represents the closed–loop slave transfer function matrix. Note that the hollow arrowheads represent physical connections, while the solid arrowheads represent signal connections. As depicted in the figures, the position-controlled slave manipulator is dependent upon the dynamics of the environment. In order to alleviate the closed-loop slave manipulator's dependence upon the environment, the slave controller includes local feedback of the interaction force occurring at the environment interface, as shown in Fig. 2*c*. The resulting closed-loop slave dynamics $\mathbf{G_s}$ are rendered independent of the environment impedance, as shown in Fig. 2*d*. Hashtrudi-Zaad and Salcudean [9] modified the approach of Lawrence [3] by incorporating similar feedback to achieve theoretically transparent teleoperation with three rather than four communication channels. Note that this force feedback is also required to render linear the nonlinear slave dynamics via impedance control, as subsequently described.

Given the master/human and slave/environment dynamics as previously described, the loop shaping telemanipulation architecture is obtained by combining the master/human and slave/environment subsystems with the position and force scaling matrices, $\mathbf{C_1}$ and $\mathbf{C_2}$, respectively, as shown in Fig. 3. The stability of the teleoperation loop is governed by the characteristics of the open-loop response given by:

$$\widetilde{\mathbf{G}} = \mathbf{Y}_h \mathbf{G}_m \mathbf{C}_2 \mathbf{Z}_e \mathbf{G}_s \mathbf{C}_1 \tag{2}$$

The transparency of the multivariable teleoperation loop is determined by the relative distortion between the transmitted impedance (i.e., the impedance felt by the human operator) and the actual environment impedance. The impedance transmitted to the human operator by the telemanipulation system is given by:

$$\widetilde{\mathbf{Z}}_t = \mathbf{G}_m \mathbf{C}_2 \mathbf{Z}_e \mathbf{G}_s \mathbf{C}_1 \tag{3}$$

For perfect transparency, the transmitted impedance transfer function matrix of Eq. (3) should equal the actual environment impedance, $\mathbf{Z}_e$. In practice, these matrices need only be similar within some frequency band of interest. Thus, within this band of interest, perfect transparency requires the singular values of the transmitted impedance transfer function matrix to equal those of the actual environment impedance transfer function matrix. As such, a measure of the desired multivariable performance can be given by the ratio of the respective singular values of the impedance transmitted to the human operator to those of the environment impedance:

$$\delta_i = \frac{\sigma_i[\widetilde{\mathbf{Z}}_t(j\omega)]}{\sigma_i[\mathbf{Z}_e(j\omega)]}, \quad 1 \le i \le n \tag{4}$$

where $rank(\widetilde{\mathbf{Z}}_\mathbf{t}, \mathbf{Z}_\mathbf{e}) = n$ and δ_i represents distortion in the teleoperative system. A desired bandwidth of transparency can be prescribed by ensuring that the distortion δ_i in each singular

value is less than some allowable amount of distortion Δ for a desired bandwidth of operation. For Δ= 3 dB, a prescription for good teleoperative performance can be written as:

$$\left|\delta_{\mathrm{dB},i}\right| \leq 3\,\mathrm{dB} \quad \forall\, \omega \in \Omega_t \tag{5}$$

where Ω_t is a desired bandwidth of teleoperative transparency.

The overall objective of the control architecture is to achieve the desired performance specified by Eq. (5) while ensuring the robust stability of the closed-loop system. With the introduction of a loop shaping compensator in the motion communication channel, the uncompensated open loop transfer function matrix $\widetilde{\mathbf{G}}$ and transmitted impedance $\widetilde{\mathbf{Z}}_t$ will both be linearly affected by the compensator transfer function matrix, and will thus be given respectively by:

$$\mathbf{G} = \mathbf{Y}_h \mathbf{G}_m \mathbf{C}_2 \mathbf{Z}_e \mathbf{G}_s \mathbf{C}_1 \mathbf{G}_\mathbf{c} \tag{6}$$

and

$$\mathbf{Z}_t = \mathbf{G}_m \mathbf{C}_2 \mathbf{Z}_e \mathbf{G}_s \mathbf{C}_1 \mathbf{G}_\mathbf{c} \tag{7}$$

Thus, if the loop-shaping compensator $\mathbf{G}_c$ is designed with sufficient flexibility, it can be utilized to modify the loop shape of Eq. (6) to provide sufficient stability robustness, and additionally can be utilized to modify the transmitted impedance (Eq. (7)) to address the performance specification described by Eq. (5).

Though design methods for multivariable loop shaping are less common than those available for SISO systems, some techniques are available to render the multivariable loop shaping design process tractable. Maciejowski [10] discusses several such techniques at length. In the case that the system can be sufficiently diagonalized with a coordinate transformation, a

useful technique is to pre and post multiply the system with appropriate coordinate transformations, then design an intermediate diagonal transfer function matrix compensator for each degree of freedom using SISO loop shaping techniques. The intermediate compensator is subsequently pre and post multiplied by the coordinate transformations used to diagonalize the plant, thus providing the final multivariable compensator. This technique is incorporated in the experimental implementation subsequently described.

4 Experimental Setup

4.1 Hardware

The multivariable loop shaping approach was implemented on a three degree-of-freedom scaled telemanipulation system in which the power was amplified from the user to the environment. The master manipulator, shown in Fig. 4, is a three degree-of-freedom direct drive robot with a semi-parallel five-bar linkage configuration. Kollmorgen Servodisc DC motors directly actuate each rotational degree of freedom, and Midori non-contact magnetoresistive rotary potentiometers provide position sensing for each motor. The manipulator is equipped with an ATI six-axis force/torque sensor capable of measuring forces and torques applied at its endpoint. A three degree-of-freedom stylus, connected to the loadcell, provides an interface for interaction between the manipulator and a human operator. The manipulator has an approximate endpoint cubic workspace measuring 0.2 m per side, and is capable of continuous endpoint forces of approximately 10 N (depending on endpoint location in the workspace). Further detail regarding the design of the master manipulator can be found in Perry [11]. The slave manipulator is a Unimate PUMA 560, shown in Fig. 5. The PUMA is a three degree-of-freedom harmonic-drive manipulator with a three degree-of-freedom wrist attached at its endpoint. The PUMA is

equipped with encoders and potentiometers for joint angle measurements, in addition to an ATI six-axis force/torque sensor, attached at the wrist, to measure forces and torques applied at the robot endpoint. The PUMA is a well-characterized industrial manipulator that has been utilized in numerous robotic research and industrial applications. Due to the fact that the master manipulator is a three degree-of-freedom robot, the wrist on the PUMA was immobilized, so that both manipulators were characterized by three degree-of-freedom spatial motion. Finally, the wrist of the PUMA was rigidly connected to a compliant structure, which provided for a three degree-of-freedom coupled environment stiffness, which was experimentally measured as:

$$F_e = \begin{bmatrix} 55 & 154 & -56 \\ -55 & 214 & 155 \\ 276 & 42 & 148 \end{bmatrix} X_e \tag{8}$$

where the elements of the stiffness matrix are in units of Newtons per meter.

4.2 Master and slave manipulator impedance control

The techniques employed in the proposed loop shaping approach require linear system dynamics of each block depicted in Fig. 3. Since robot manipulators are generally characterized by nonlinear dynamics, impedance control can be utilized on both manipulators to impose a desired linear dynamics on the endpoints of each. The equations of motion for the master and slave manipulators can be expressed in the following general form:

$$\tau_{\mathrm{m}} = \mathbf{I}_m(q_{\mathrm{m}})\ddot{q}_{\mathrm{m}} + \mathrm{V}_{\mathrm{m}}(q_{\mathrm{m}}, \dot{q}_{\mathrm{m}}) + \mathrm{G}_{\mathrm{m}}(q_{\mathrm{m}}) + \mathbf{J}_{\mathrm{m}}^{\mathrm{T}}(q_{\mathrm{m}})F_{\mathrm{mh}} \tag{9}$$

$$\tau_{\mathrm{s}} = \mathbf{I}_s(q_{\mathrm{s}})\ddot{q}_{\mathrm{s}} + \mathrm{V}_{\mathrm{s}}(q_{\mathrm{s}}, \dot{q}_{\mathrm{s}}) + \mathrm{G}_{\mathrm{s}}(q_{\mathrm{s}}) - \mathbf{J}_{\mathrm{s}}^{\mathrm{T}}(q_{\mathrm{s}})F_{\mathrm{e}} \tag{10}$$

where the subscript *m* refers to the master, the subscript *s* refers to the slave, q is the vector of the three generalized joint coordinates, $\mathbf{I}(q)$ represents the inertia matrix, $\mathrm{V}(q, \dot{q})$ is a vector

comprising the torques due to Coriolis and centrifugal accelerations, G(q) represents the vector of torques due to the acceleration of gravity, τ is the vector of joint torques applied to the three rotational degrees of freedom, $\mathbf{J}^{\mathrm{T}}(q)$ is the transpose of the Jacobian matrix, F_{mh} is the vector of external forces exerted by the endpoint of the master on the human operator, and F_e is the vector of forces exerted by the external environment on the endpoint of the slave. The matrix definitions and parameters for the master model (Eq. (9)) are given in [11]. The matrix definitions and parameters for the slave model (Eq. (10)) were obtained from Armstrong et al. [12], who derived the model of the dynamics of the PUMA 560 arm and measured the parameters necessary to implement model-based control. The respective impedance controllers, derived using the methodology of Hogan [13], are given by:

$$\tau_m = \mathbf{I}_m(q_m)\mathbf{J}_m^{-1}(q_m)\left[\ddot{X}_{h,d} - \frac{d}{dq_m}\left[\mathbf{J}_m(q_m)\dot{q}_m\right]\dot{q}_m\right] + \mathrm{V}_m(q_m,\dot{q}_m) + \mathrm{G}_m(q_m) + \mathbf{J}_m^T(q_m)F_{mh} \quad (11)$$

$$\tau_s = \mathbf{I}_s(q_s)\mathbf{J}_s^{-1}(q_s)\left[\ddot{X}_{s,d} - \frac{d}{dq_s}\left[\mathbf{J}_s(q_s)\dot{q}_s\right]\dot{q}_s\right] + \mathrm{V}_\mathrm{s}(q_\mathrm{s},\dot{q}_\mathrm{s}) + \mathrm{G}_\mathrm{s}(q_\mathrm{s}) - \mathbf{J}_\mathrm{s}^{\mathrm{T}}(q_\mathrm{s})F_\mathrm{e} \quad (12)$$

where $\ddot{X}_{h,d}$ defines the desired endpoint force-control dynamics of the master manipulator and $\ddot{X}_{s,d}$ determines the endpoint position-control dynamics of the PUMA. The desired endpoint behaviors for the master and slave endpoints are specified by:

$$\ddot{X}_{h,d} = \mathbf{M}_m^{-1}\left(F_h - F_{mh}\right) \quad (13)$$

$$\ddot{X}_{s,d} = \mathbf{M}_s^{-1}\left[\mathbf{K}_s(X_e - X_s) - \mathbf{B}_s\dot{X}_s\right] \quad (14)$$

where $\mathbf{M}_m$ is a diagonal matrix of masses, F_h is the vector of desired forces to be imposed by the master manipulator on the human operator, F_{mh} is the vector of forces exerted by the master manipulator on the human operator, $\mathbf{M}_\mathrm{s}$ is a diagonal matrix of masses, $\mathbf{K}_\mathrm{s}$ is a diagonal stiffness matrix, $\mathbf{B}_\mathrm{s}$ is a diagonal damping matrix, and X_e is the scaled position command from the human

operator. The master manipulator behaves as a mass system in response to the summation of the forces imposed by the human operator with those commanded from the teleoperated slave/environment interaction. Note that for the case where the desired vector of forces (F_h) is zero, the manipulator is controlled to behave as a pure inertia in response to forces arising from the interaction with the human operator (F_{mh}). The imposed behavior of the endpoint of the PUMA is specified, in each degree of freedom, as a mass under proportional plus derivative control. The matrices governing the endpoint behaviors of the master and slave are given numerically by:

$$\mathbf{M}_m = \begin{bmatrix} 1\,kg & 0 & 0 \\ 0 & 1\,kg & 0 \\ 0 & 0 & 1\,kg \end{bmatrix} \qquad \mathbf{M}_s = \begin{bmatrix} 1\,kg & 0 & 0 \\ 0 & 1\,kg & 0 \\ 0 & 0 & 1\,kg \end{bmatrix}$$

$$\mathbf{B}_s = \begin{bmatrix} 45\,\frac{Ns}{m} & 0 & 0 \\ 0 & 45\,\frac{Ns}{m} & 0 \\ 0 & 0 & 89\,\frac{Ns}{m} \end{bmatrix} \qquad \mathbf{K}_s = \begin{bmatrix} 1000\,\frac{N}{m} & 0 & 0 \\ 0 & 1000\,\frac{N}{m} & 0 \\ 0 & 0 & 4000\,\frac{N}{m} \end{bmatrix} \tag{15}$$

Note that $\mathbf{M}_m$, $\mathbf{M}_s$, $\mathbf{B}_s$, and $\mathbf{K}_s$ need not be diagonal, but there is no reason to specify them otherwise.

4.3 Experimental measurement of transparency

Characterization of the experimental transparency exhibited by the teleoperation loop, as described by Eq. (4), requires measurement of both the environment impedance and the transmitted impedance. Since the transparency depends on the relative values of the transmitted and actual environment impedance, the multivariable transparency can be assessed by measurement of the dynamic stiffness (i.e., the dynamic relationship between force and displacement) rather than direct measurement of the impedance. The former is preferable

because it provides matrix elements with nonzero DC gains, and thus most likely provides a more accurate measurement. Thus, the transparency is assessed by experimental determination of the environment and transmitted dynamic stiffness matrices, which for the three degree-of-freedom system are of the form:

$$\begin{bmatrix} F_x \\ F_y \\ F_z \end{bmatrix} = \begin{bmatrix} k_{11}(\omega) & k_{12}(\omega) & k_{13}(\omega) \\ k_{21}(\omega) & k_{22}(\omega) & k_{23}(\omega) \\ k_{31}(\omega) & k_{32}(\omega) & k_{33}(\omega) \end{bmatrix} \begin{bmatrix} x \\ y \\ z \end{bmatrix} \tag{16}$$

where $k_{ij}(\omega)$ represent the nine components of the dynamic stiffness as a function of excitation frequency. Identification of the environment transfer function matrix uses the positions (X_e) and corresponding forces (F_e) of the slave/environment interaction, while identification of the transmitted transfer function matrix uses the positions (X_h) and forces (F_{mh}) occurring at the master/human interface. Colgate [14] experimentally measured a similar multivariable transfer function matrix, and an analogous methodology is used here to compute the transfer function matrices needed to assess the teleoperation loop's transparency. Specifically, the human operator provided voluntary excitation of the teleoperation loop at several frequencies. For each excitation frequency, the operator commanded motion separately in each degree of freedom. The positions and interaction forces corresponding to the environment dynamic stiffness and transmitted dynamic stiffness were measured for each degree of freedom and excitation frequency. The respective transfer function matrices were then computed from the measured data.

Consider the computation of the environment dynamic stiffness for human voluntary motion along the *x*-axis. At each excitation frequency, the following auto- and cross-power

spectral densities are computed: $\Phi_{x_s x_s}(\omega)$, $\Phi_{x_s y_s}(\omega)$, $\Phi_{x_s z_s}(\omega)$, $\Phi_{x_s F_{e,x}}(\omega)$, $\Phi_{x_s F_{e,y}}(\omega)$, and $\Phi_{x_s F_{e,z}}(\omega)$. From these spectral densities, the following transfer functions are computed:

$$G_{e,1x}(\omega) = \frac{\Phi_{x_s F_{e,x}}(\omega)}{\Phi_{x_s x_s}(\omega)} \tag{17}$$

$$G_{e,2x}(\omega) = \frac{\Phi_{x_s F_{e,y}}(\omega)}{\Phi_{x_s x_s}(\omega)} \tag{18}$$

$$G_{e,3x}(\omega) = \frac{\Phi_{x_s F_{e,z}}(\omega)}{\Phi_{x_s x_s}(\omega)} \tag{19}$$

$$H_{e,1x}(\omega) = \frac{\Phi_{x_s y_s}(\omega)}{\Phi_{x_s x_s}(\omega)} \tag{20}$$

$$H_{e,2x}(\omega) = \frac{\Phi_{x_s z_s}(\omega)}{\Phi_{x_s x_s}(\omega)} \tag{21}$$

where $G_{e,1x}(\omega)$, $G_{e,2x}(\omega)$, and $G_{e,3x}(\omega)$ are transfer functions relating the x_s-axis excitation to the interaction forces in each degree of freedom (i.e., $F_{e,x}$, $F_{e,y}$, and $F_{e,z}$), and $H_{e,1x}(\omega)$ and $H_{e,2x}(\omega)$ are transfer functions relating the primary x_s-axis excitation to those in the y_s- and z_s-axes. Analogous methods are used to compute the complementary sets of transfer functions governing the human excitations of the loop along the y_s- and z_s-axes. From these transfer functions, the components of the environment dynamic stiffness matrix can be computed using:

$$\begin{bmatrix} k_{e,11} \\ k_{e,12} \\ k_{e,13} \\ k_{e,21} \\ k_{e,22} \\ k_{e,23} \\ k_{e,31} \\ k_{e,32} \\ k_{e,33} \end{bmatrix} = \begin{bmatrix} 1 & H_{e,1x} & H_{e,2x} & 0 & 0 & 0 & 0 & 0 & 0 \\ 0 & 0 & 0 & 1 & H_{e,1x} & H_{e,2x} & 0 & 0 & 0 \\ 0 & 0 & 0 & 0 & 0 & 0 & 1 & H_{e,1x} & H_{e,2x} \\ H_{e,1y} & 1 & H_{e,2y} & 0 & 0 & 0 & 0 & 0 & 0 \\ 0 & 0 & 0 & H_{e,1y} & 1 & H_{e,2y} & 0 & 0 & 0 \\ 0 & 0 & 0 & 0 & 0 & 0 & H_{e,1y} & 1 & H_{e,2y} \\ H_{e,1z} & H_{e,2z} & 1 & 0 & 0 & 0 & 0 & 0 & 0 \\ 0 & 0 & 0 & H_{e,1z} & H_{e,2z} & 1 & 0 & 0 & 0 \\ 0 & 0 & 0 & 0 & 0 & 0 & H_{e,1z} & H_{e,2z} & 1 \end{bmatrix}^{-1} \begin{bmatrix} G_{e,1x} \\ G_{e,2x} \\ G_{e,3x} \\ G_{e,1y} \\ G_{e,2y} \\ G_{e,3y} \\ G_{e,1z} \\ G_{e,2z} \\ G_{e,3z} \end{bmatrix} \quad (22)$$

The components of the transmitted dynamic stiffness matrix are obtained in a comparable manner, using the experimental position and force data associated with the teleoperative interaction between the human operator and master manipulator. The singular values of the dynamic stiffness matrices can then be computed from these matrices. The ratios of the singular values of the dynamic stiffness matrices are equal to the ratios of the singular values of the respective impedances. Thus, the measure of transparency described by Eq. (4) is obtained.

5 Experimental Results

5.1 Transparency and stability robustness of the uncompensated system

The teleoperation control architecture with the environment force feedback shown in Fig. 2*c* and the impedance controllers described by Eqs. (11-15) was implemented, initially without a loop shaping compensator, with the real-time interface provided by MATLAB/Simulink (The Mathworks, Inc.) at a sampling rate of 1 kHz. The position and force scaling matrices used in the experimental telemanipulator are given by:

$$\mathbf{C}_1 = \begin{bmatrix} 2 & 0 & 0 \\ 0 & 2 & 0 \\ 0 & 0 & 2 \end{bmatrix} \tag{23}$$

$$\mathbf{C}_2 = \begin{bmatrix} 0.5 & 0 & 0 \\ 0 & 0.5 & 0 \\ 0 & 0 & 0.5 \end{bmatrix} \tag{24}$$

where $\mathbf{C}_1$ is the matrix that scales the slave position commands, and $\mathbf{C}_2$ is the matrix governing the scaling of the master force commands. As such, the telemanipulator was operated as a man-amplifier (i.e., the power exerted by the slave was four times the power exerted by the human). To assess the transparency of the loop, the human provided periodic motion in each degree of freedom for five different frequencies: 0.25 Hz, 0.5 Hz, 1 Hz, 2 Hz, and 4 Hz. Voluntary excitation of the system at frequencies above 4 Hz proved to lie beyond the bandwidth of human gross motor capability. The temporal data of the voluntary excitation was used as visual feedback in order for the human to accurately command the desired frequency of excitation. Five successive trials were conducted for each data point (i.e., for each degree of freedom and excitation frequency), and the resulting singular values averaged across the five trials.

Fig. 6 shows the transparency distortion, as defined by Eq. (4), averaged across the five trials, corresponding to each singular value in the transmitted impedance. If the extent of allowable distortion is defined as Δ= 3 dB, then the transparency bandwidth can be defined as the lowest frequency at which the transparency distortion exceeds ±3 dB. For the uncompensated system, the transparency bandwidth exhibited by the teleoperator loop is approximately 0.5 Hz, as determined by the minimum singular value in Fig. 6.

Stability robustness of the multivariable loop was initially assessed using the singular values computed from the open-loop transfer function matrix and the notions of multiplicative and divisive uncertainty, as respectively described by Doyle and Stein [15] and Lehtomaki et al. [16]. This approach, however, proved too sensitive to sensor noise and unmodeled dynamics to provide any useful insights. Specifically, the approach indicated stability robustness when the corresponding closed loop was in fact quite unstable. As such, a direct measure of the stability robustness was obtained by measuring the average power output to the human operator at various loop gains. For these measurements, the human operator provided pseudo-random excitation simultaneously in all three degrees of freedom. Instability in the teleoperation loop was indicated by positive average power output to the human operator, as well as uncontrollable oscillatory behavior of the system. Fig. 7*a* shows the instantaneous power (solid line) and moving-average power (dashed line) for teleoperative interaction with the original environment impedance. Note that the moving-average power at each time step was computed using a window two seconds in length. The results of Fig. 7*a* show that teleoperative interaction with the original environment impedance is stable, with zero or negative average power output to the human. Fig. 7*b* depicts the results for the teleoperation loop with an increase in the scaling gain by a factor of 1.1 in each channel. This marginal increase in the loop gain caused the system to exhibit significant instability in the form of sustained uncontrollable oscillation in each degree of freedom, and additionally manifested as positive average power output in each degree of freedom. As such, the data shown in Fig. 7*b* would indicate that the teleoperator loop becomes unstable at a gain of 1.1 in each channel, and thus has an effective gain margin of less than 0.8 dB in each degree-of-freedom. Thus, in summary, the teleoperation loop without loop-shaping

compensation exhibits a transparency bandwidth of approximately 0.5 Hertz and essentially no stability robustness.

5.2 Transparency and stability robustness of the compensated system

A multivariable loop shaping compensator was designed for this system by incorporating a coordinate transformation to approximately decouple the coupled teleoperation loop (which is coupled through the environment behavior as described by Eq. (8)). Though not perfect in decoupling the telemanipulation loop, the coordinate transformation does reorient the reference frame for the compensator such that the transformed system exhibits diagonally dominant behavior. Following the coordinate transformation, frequency-domain compensation was implemented in each approximately decoupled degree of freedom. In particular, lead compensation implemented in each degree of freedom proved an effective means for obtaining improved stability robustness while also shaping the impedance transmitted to the human operator. The complete multivariable loop shaping compensator was obtained by pre and post multiplying the diagonal loop-shaping matrix with the decoupling matrix and its inverse, respectively, such that

$$\mathbf{G}_c = \begin{bmatrix} 0.5 & 0.71 & -0.5 \\ -0.5 & 0.71 & 0.5 \\ 0.71 & 0 & 0.71 \end{bmatrix} \begin{bmatrix} 1.3\left(\dfrac{1.7s+8}{s+8}\right) & 0 & 0 \\ 0 & \dfrac{1.3s+15}{s+15} & 0 \\ 0 & 0 & \dfrac{4.6s+80}{s+80} \end{bmatrix} \begin{bmatrix} 0.5 & -0.5 & 0.71 \\ 0.71 & 0.71 & 0 \\ -0.5 & 0.5 & 0.71 \end{bmatrix} \quad (25)$$

which yields the multivariable compensator:

$$\mathbf{G_c} = \frac{\mathbf{N_c}}{D_c} \quad (26)$$

where

$$\mathbf{N_c} = \begin{bmatrix} 2.4s^3 + 166s^2 + 2580s + 10320 & -1.1s^3 - 37s^2 - 432s - 720 & -0.85s^3 + 12.25s^2 + 443s + 1020 \\ -1.1s^3 - 37s^2 - 432s - 720 & 2.4s^3 + 166s^2 + 2580s + 10320 & 0.85s^3 - 12.25s^2 - 443s - 1020 \\ -0.85s^3 + 12.25s^2 + 443s + 1020 & 0.85s^3 - 12.25s^2 - 443s - 1020 & 3.4s^3 + 203s^2 + 3016s - 11040 \end{bmatrix} \quad (27)$$

and

$$D_c = s^3 + 103s^2 + 1960s + 9600 \quad (28)$$

This loop shaping compensator was added to the previously uncompensated system. Using the methodology previously described, the transparency distortion of the teleoperation loop with the compensator of Eqs. (26-28) was measured as shown in Fig. 8. As indicated in the figure, the addition of the loop-shaping compensation increased the transparency bandwidth exhibited by the loop to approximately 2.7 Hz, which is more than a factor of five improvement relative to the uncompensated case.

Fig. 9*a* shows the instantaneous (solid line) and moving-average (dashed line) power output in each degree of freedom for an increase in the loop gain by a factor of 1.9. For this case, the compensated system exhibited stable behavior with zero or negative average power output in each degree of freedom, in addition to the absence of any sustained oscillations. The plots of Fig. 9*b* show the power output of the telemanipulator system for a factor of two increase in the loop gain. The system exhibited sustained oscillation and positive power output to the human operator for this case. Thus the compensated loop can be characterized by a gain margin of approximately 6.0 dB in each degree-of-freedom. Relative to the uncompensated system, the introduction of a loop shaping compensator increased the transparency bandwidth by more than a factor of five and increased the gain margin by a factor of approximately two (i.e., by approximately six decibels per channel).

6 Conclusions

A previously proposed method of obtaining transparency and stability in bilateral teleoperation was extended here to accommodate multivariable systems. The approach was experimentally demonstrated on a three degree-of-freedom scaled telemanipulator pair that incorporated nonlinear manipulators and a highly coupled environment. Using direct measurement of the power delivered to the operator to assess the system's stability robustness, along with the proposed measure of multivariable transparency, the loop-shaping compensation was shown to improve the stability robustness by a factor of two and the transparency by more than a factor of five.

References

[1] Hannaford, B., 1989. "A Design Framework for Teleoperators with Kinesthetic Feedback." *IEEE Transactions on Robotics and Automation*, Vol. 5, No. 4, pp. 426-434.

[2] Yokokohji, Y. and Yoshikawa, T., 1992. "Bilateral Control of Master-Slave Manipulators for Ideal Kinesthetic Coupling." *Proceedings of the IEEE Conference on Robotics and Automation*, pp. 849-858.

[3] Lawrence, D.A., 1993. "Stability and Transparency in Bilateral Telemanipulation." *IEEE Transactions on Robotics and Automation*, Vol. 9, No. 5, pp. 624-637.

[4] Colgate, J. E., 1993. "Robust Impedance Shaping Telemanipulation." *IEEE Transactions on Robotics and Automation*, Vol. 9, No. 4, pp. 374-384.

[5] Itoh, T., Kosuge, K., and Fukuda, T., 2000. "Human-Machine Cooperative Telemanipulation with Motion and Force Scaling Using Task-Oriented Virtual Tool Dynamics." *IEEE Transactions on Robotics and Automation*, Vol. 16, No. 5, pp. 505-516.

[6] Hashtrudi-Zaad, K. and Salcudean, S. E., 2002. "Bilateral Parallel Force/Position Teleoperation Control." *Journal of Robotic Systems*, Vol. 19, No. 4, pp. 155-167.

[7] Doyle, J. C., 1982. "Analysis of Feedback Systems with Structured Uncertainties." *Proceedings of IEE, Part D*, Vol. 129, No. 6, pp. 242-250.

[8] Fite, K.B., Speich, J.E., and Goldfarb, M., 2001. Transparency and Stability Robustness in Two-Channel Bilateral Telemanipulation. *ASME Journal of Dynamic Systems, Measurement, and Control*, Vol. 123, No. 3, pp. 400-407.

[9] Hashtrudi-Zaad, K. and Salcudean, S. E., 1999. "On the Use of Local Force Feedback for Transparent Teleoperation." *Proceedings of the IEEE Conference on Robotics and Automation*, pp. 1863-1869.

[10] Maciejowski, J. M., 1989. *Multivariable Feedback Design*. Addison-Wesley. Reading, MA.

[11] Perry, C.M., 1997. "Design of a High Performance Robot for use in Haptic Interface and Force Feedback Research." Master's Thesis, Department of Mechanical Engineering, Vanderbilt University.

[12] Armstrong, B., Khatib, O., and Burdick, J., 1986. "The Explicit Dynamic Model and Inertial Parameters of the PUMA 560 Arm." *Proceedings of the IEEE International Conference on Robotics and Automation*, pp. 510-518.

[13] Hogan, N., 1985. "Impedance Control: An Approach to Manipulation: Parts I-III." *ASME Journal of Dynamic Systems, Measurement, and Control*, Vol. 107, No. 1, pp. 1-24.

[14] Colgate, J. E., 1994. "Coupled Stability of Multiport Systems—Theory and Experiments." *ASME Journal of Dynamic Systems, Measurement, and Control*, Vol. 116, No. 3, pp. 419-428.

[15] Doyle, J. C., and Stein, G., 1981. "Multivariable Feedback Design: Concepts for a Classical/Modern Synthesis." *IEEE Transactions on Automatic Control*, Vol. 26, No. 1, pp. 4-16.

[16] Lehtomaki, N. A., Sandell, N. R., and Athans, M., 1981. "Robustness in Linear-Quadratic Gaussian Based Multivariable Control Designs." *IEEE Transactions on Automatic Control*, Vol. 26, No. 1, pp. 75-93.

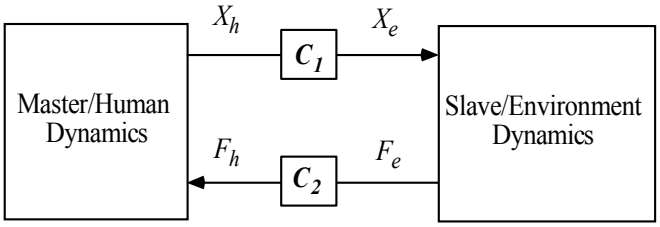

Fig. 1. General two-channel bilateral telemanipuation system.

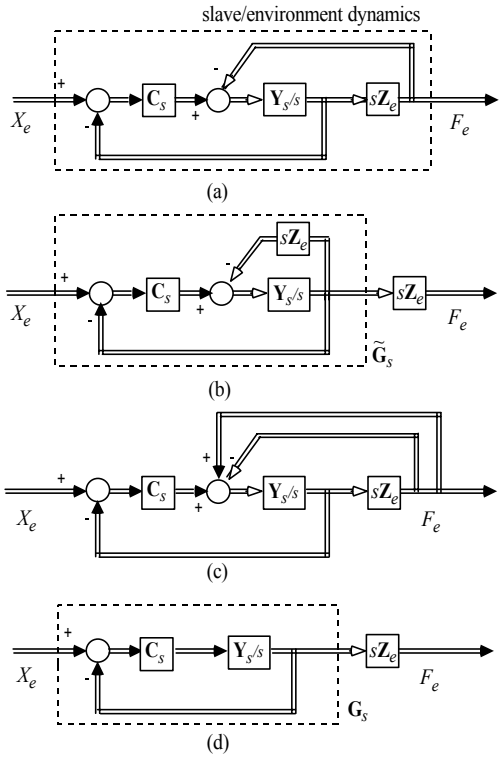

Fig. 2. Multivariable slave/environment dynamics: (a) Schematic of closed-loop position-controlled slave manipulator interacting with environment impedance; (b) Restructuring of interaction to clearly show the closed-loop slave's dependence on $\mathbf{Z}_e$; (c) Inclusion of local feedback to decouple $\mathbf{G}_s$ from $\mathbf{Z}_e$; and (d) Schematic of resulting dynamics.

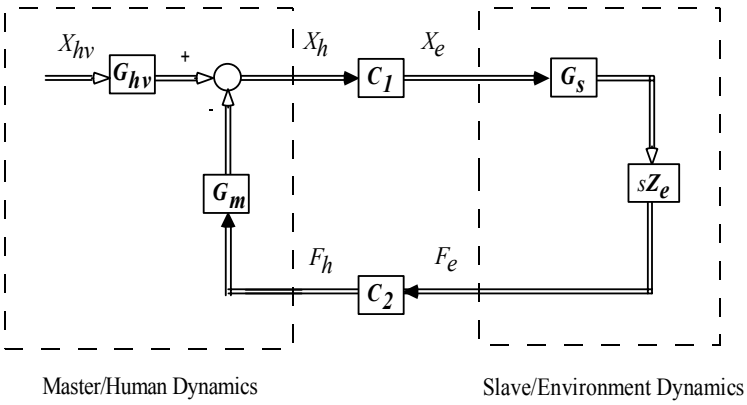

Fig. 3. Multivariable bilateral telemanipulation system.

Fig. 4. Three degree-of-freedom master manipulator.

Fig. 5. Unimate PUMA 560 robot manipulator.

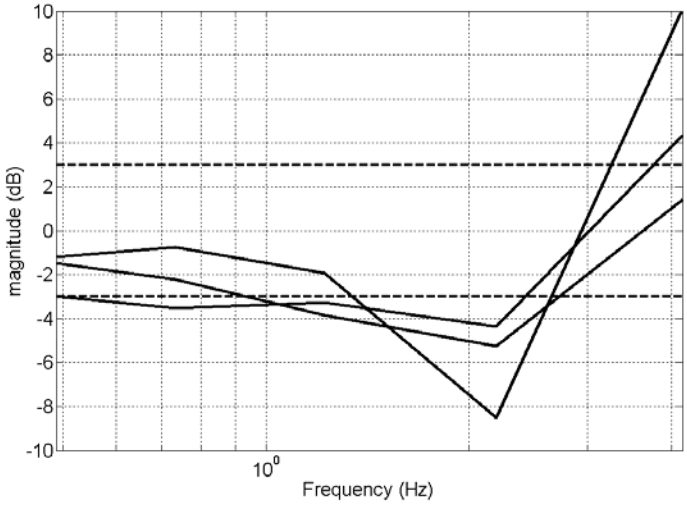

Fig. 6. Transparency distortion corresponding to each singular value in the transmitted impedance for the uncompensated system. The dashed lines indicate the ±3 dB desired performance specification.

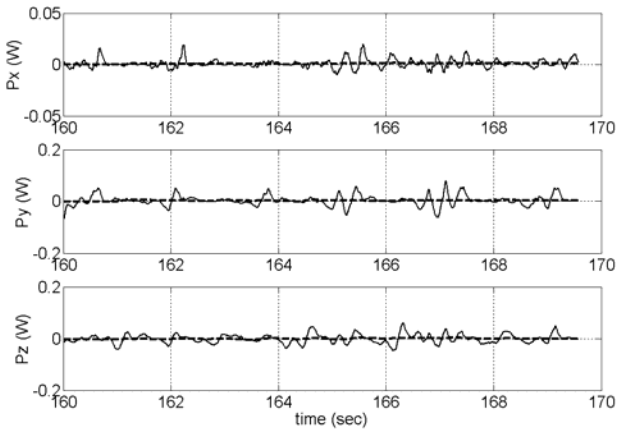

(a)

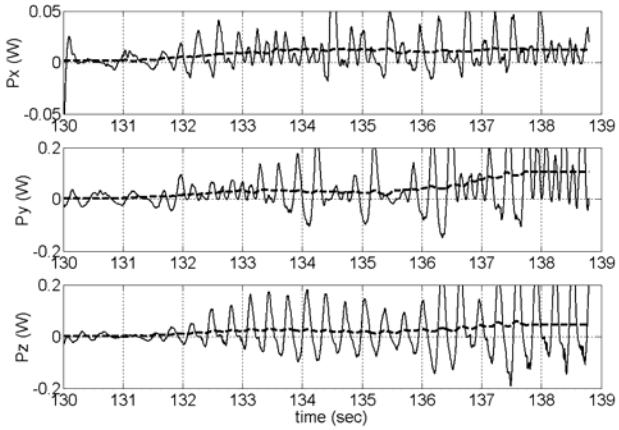

(b)

Fig. 7. Instantaneous power (solid line) and moving-average power (dashed line) output to the human: (a) uncompensated teleoperation with the original environment impedance; (b) uncompensated teleoperation with the environment impedance scaled by 1.1.

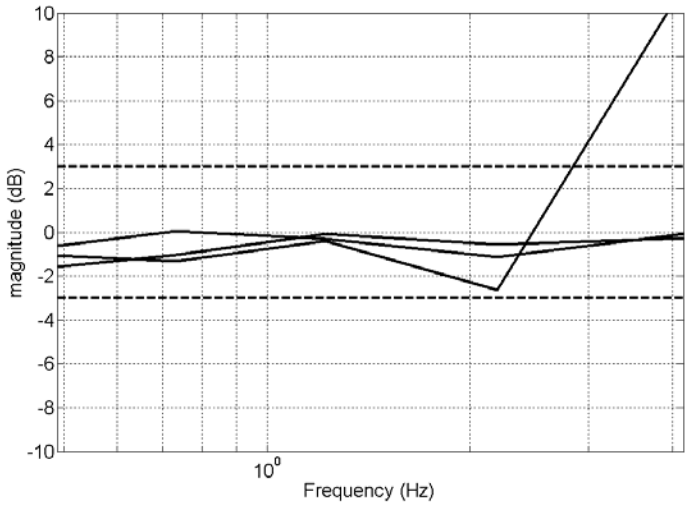

Fig. 8. Transparency distortion corresponding to each singular value in the transmitted impedance for the compensated system. The dashed lines indicate the ±3 dB desired performance specification.

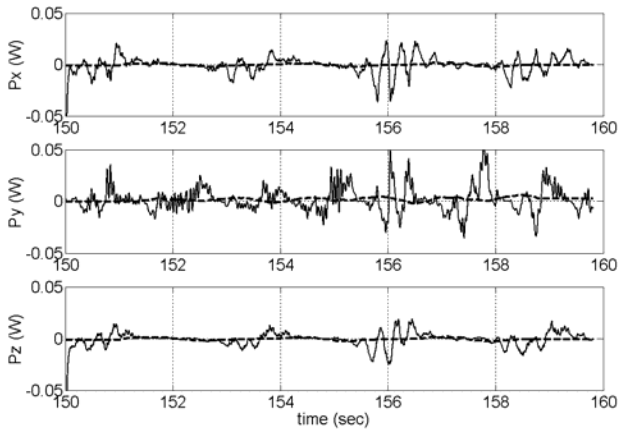

(a)

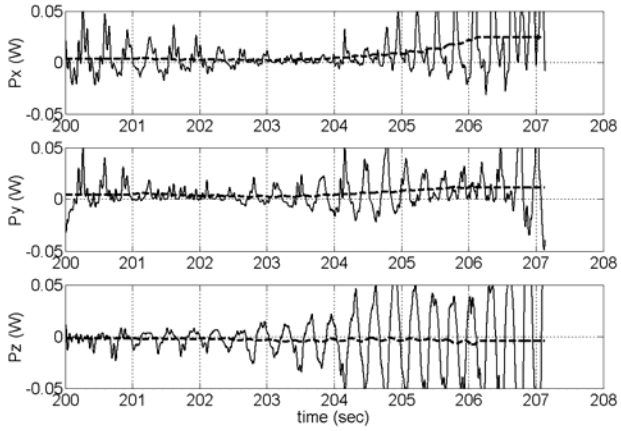

(b)

Fig. 9. Instantaneous power (solid line) and moving-average power (dashed line) output to the human: (a) compensated teleoperation with the environment impedance scaled by 1.9; (b) compensated teleoperation with the environment impedance scaled by 2.